Vibro-acoustic Prediction Model for Impact Sound Insulation of Cross-laminated Timber

Melanie F. Gotfredsen[1,2], Julie B. Liengaard [1,3], Christoffer A. Weitze [2], Jonas Brunskog[1]
[1] *Technical University of Denmark, 2800 Kgs. Lyngby, Denmark*
[2] *NIRAS A/S, 3450 Lillerød, Denmark*
[3] *FORCE Technology, 2970 Hørsholm, Denmark*

Introduction

Sustainability awareness has increased the use of lightweight materials in the building industry, though these are often associated with poor sound insulation [1, 2]. Cross-laminated timber (CLT) is a favoured lightweight material due to its customizability and load-bearing capacity. However, meeting acoustical, fire-safety, and other technical requirements often involves additional materials, reducing its sustainability benefits.

Current prediction models rely on empirical data, requiring extensive laboratory testing, which is time-consuming and resource-intensive. This study explores a computational prediction model independent of empirical data as part of a larger master's thesis project [3].

CLT Floor Specimen

Two CLT panels were joined with 35 evenly spaced 240 mm screws into a 10 m^2 CLT floor specimen (2.98 × 3.34 × 0.24 m). It consisted of seven orthogonally oriented layers with thicknesses 4-2-4-4-4-2-4 cm. The floor's density was measured to be 460.4 kg/m^3, giving a surface mass of 110.5 kg/m^2. A picture of the floor is presented in Figure 1.

Figure 1: The CLT test specimen.

Research Approach

Simulating the impact sound insulation of CLT is a complicated task, and one has to be very careful with the model's inputs. Hence the project was subdivided into three main tasks, the first two focusing on correctly determining the input parameters:

- Determining CLT mechanical properties.
- Simulating the excitation force spectrum of a tapping machine.
- Simulating CLT impact sound insulation using the obtained parameters.

Determining Mechanical Properties

Mechanical properties were determined through a longitudinal wave speed experiment and a literature review. Computational and experimental modal analyses were compared using the modal assurance criterion (MAC) to identify the best-fit parameters. Two boundary conditions (BCs) were considered: simply supported at eight points and in the laboratory test-opening. Brass cones (5 cm high, 1 cm top diameter, 5 cm bottom diameter) were used to approximate the simply supported points, with supports placed at each panel corner.

Longitudinal Wave Speed Experiment

The floor was simply supported and excited with an impact hammer, while an accelerometer measured the response on the opposite side in the same layer, aligned with the stiffest direction (parallel to grain). The wave travelled 2.98 m in 0.66 ms, yielding a longitudinal wave speed of 4515 m/s. Using

$$E = c_L^2 \rho (1 - \nu^2), \tag{1}$$

with previously measured density (460.4 kg/m^3) and assuming Poisson's ratio to be 0.3, the initial Young's modulus estimate in the stiffest direction (E_L) was calculated to be 8.5 GPa.

Mechanical Properties from Literature

The estimated E_L was compared to literature values. The *Wood Handbook* [4] reported an E_L range of 9–11.3 GPa, slightly higher than the estimate. Otani et al. [5] provided a broader range of 6–18 GPa for softwood. Additional mechanical properties were scaled based on E_L in both references. Four combinations from these sources were selected for computational analysis (Table 1).

Table 1: Mechanical properties of CLT used in computational modal analyses.

Mechanical Property	Wood Handbook		Otani et al.	
	10.5 GPa	12 GPa	8 GPa	11 GPa
$\mathbf{E}_L$	10.5	12	8	11
$\mathbf{E}_T$	0.45	0.52	0.79	0.89
$\mathbf{E}_R$	0.82	0.94	0.45	0.55
$\mathbf{G}_{LT}$	0.67	0.77	0.70	0.76
$\mathbf{G}_{TR}$	0.64	0.73	0.65	0.71
$\mathbf{G}_{LR}$	0.03	0.04	0.06	0.07

Modal Analyses and Modal Assurance Criterion
Modal analyses were performed both experimentally and computationally. The experimental setup, illustrated in Figure 2, involved exciting the floor at two positions using a Brüel & Kjær vibration exciter and measuring responses at 30 grid points with an accelerometer. Frequency response functions (FRFs) were averaged at each grid point, yielding 30 FRFs. Resonance frequencies were identified manually, and mode shapes were visualized using linear interpolation, as shown in Figure 3. Computationally, mode shapes and natural frequencies were determined via COMSOL Multiphysics' eigenfrequency study, with results presented in Figure 4. The same procedure was applied to the floor inserted in the laboratory test-opening, referred to as *in-frame*.

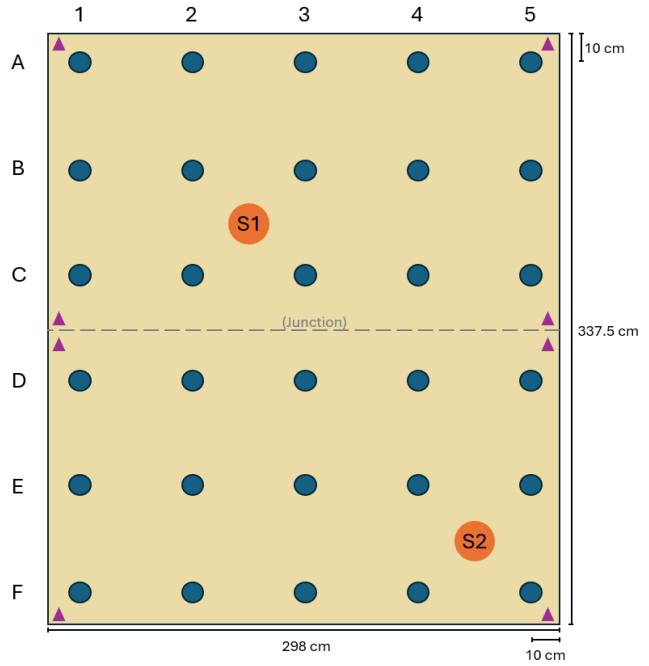

Figure 2: Sketch of the measurement (blue) and excitation (orange) positions for the modal analysis measurements. As well as the location of the junction (grey dashed line). The simply supports were located approx. 5 cm from each corner of each CLT element (purple triangles). The edge of the measurement grid was 10 cm from the floor's edge, and the additional measurement positions were uniformly distributed between these points.

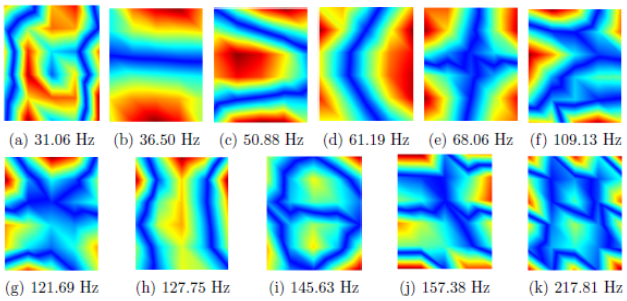

Figure 3: The first 11 modes found from the measured FRFs of the simply supported floor (xy-plane view).

The measured and computed mode shapes were compared using the MAC, given by

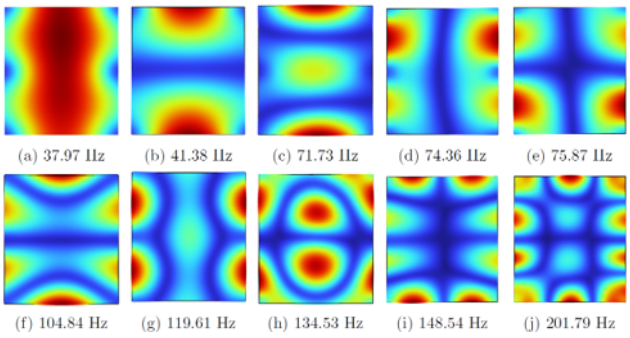

Figure 4: The first 10 modes found from the computed FRFs of the simply supported floor (xy-plane view).

$$MAC = \frac{\left|\Psi_m^T \Psi_c^*\right|^2}{\Psi_m^T \Psi_m^* \Psi_c^T \Psi_c^*}, \tag{2}$$

where Ψ_m and Ψ_m are the measured and computed modal vectors, respectively.The modal vectors were derived from the FRF at resonance frequencies, with each grid point serving as an element in the vector. For computed mode shapes, displacements at the same grid points were used to generate the modal vector. Using the mechanical properties from Otani et al. ($E_L = 8.5$ GPa), the MAC identified the best fit to the measured modal vector, as shown in Figure 5. The diagram reveals a clear diagonal trend with values nearing unity, indicating comparable computed and measured mode shapes. The ideal MAC diagram would present a diagonal line with values of 1 and elsewhere zero, however this is not realistic to obtain.

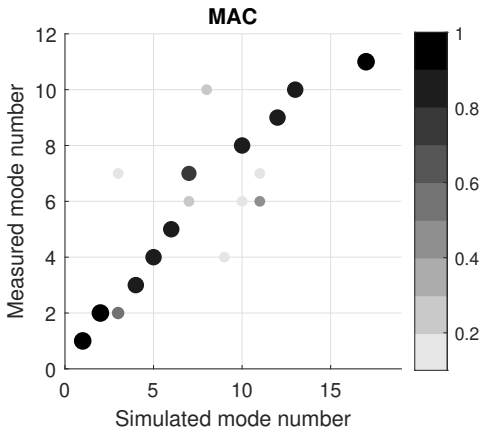

Figure 5: Modal assurance criterion values for every combination of measured and computed modes, using the material properties given in [5] with E_L being 8 GPa.

The floor in-frame underwent the same exercise; however, the laboratory frame's boundary conditions were inadequately modelled. Figure 6 displays the MAC diagram with the highest values for in-frame. Unlike the previous case, no clear diagonal trend is observed, and the values are notably low, indicating poor comparability between the measured and computed mode shapes in-frame.

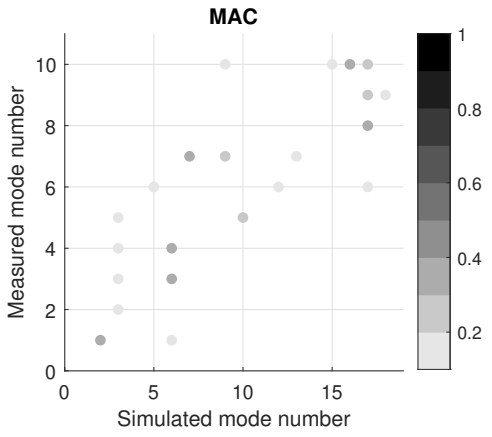

Figure 6: Modal assurance criterion values for every combination of measured and computed modes for the floor in-frame. Modelled BCs was a periodic fixed-free line with 5 cm offset from the edge.

Simulating the excitation force spectrum

In [6] the force spectrum from the standard tapping machine was investigated and the repeated force spectrum was expressed as

$$F_R(f) = \sum_{n=-\infty}^{\infty} F_n \delta(f - n f_r), \tag{3}$$

where f is the frequency, f_r is the repetition frequency of the tapping machine (10 Hz) and each amplitude, F_n, is given by

$$F_n = 1/T_r \int_0^{T_r} f_1(t) e^{-i2\pi n t/T_r}, \tag{4}$$

where T_r is the repetition period of the tapping machine, f_1 is one impact pulse from one hammer and n is an integer. Meaning that the repeated impact force spectrum can be described by a single impact of one hammer in time domain. This was simulated in COMSOL Multiphysics by modelling the CLT floor (with MAC verified mechanical properties) and model the cylindrical hammer on top of it. The hammer was given the initial velocity of 0.886 m/s in the normal direction towards the floor. This velocity was found analytically knowing the standard hammer's properties, for more information see [6]. The resulting force was obtained by taking the surface integral of the stress in the shared surface, the result can be seen in Figure 7. No damping was introduced, leading to high-frequency spurious oscillations in the beginning of the signal. Following [7], a 6000 Hz low-pass filter was applied to reduce these oscillations, although some effects remained visible at the peak. A 2500 Hz low-pass filtered signal is provided to illustrate the theoretically expected shape.

To isolate a single impact (without rebound), the signal was truncated at its first zero-crossing and zero-padded to obtain frequency components at 10 Hz intervals after Fourier transformation from Eq. 3. Figure 8 presents the resulting force spectrum for five arbitrarily chosen excitation positions. The spectrum shows minimal sensitivity

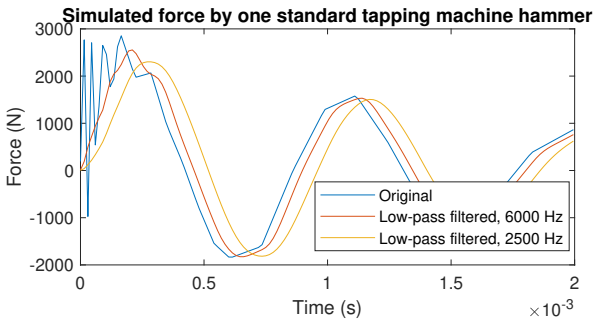

Figure 7: The simulated force's time profile for one standard tapping machine hammer, without filtering, with a low-pass filter at 6000 Hz and a low-pass filter at 2500 Hz. Note that negative values correspond to the hammer lifting itself off the floor.

to excitation position; therefore, only the force spectrum of position I was utilized in subsequent analyses. Red stars indicate the theoretical low-frequency asymptotes determined analytically (see [6] for details)

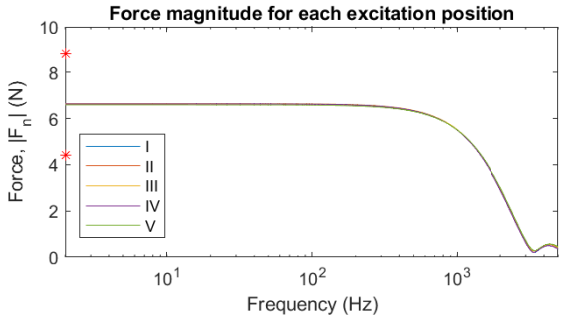

Figure 8: The simulated one-sided force magnitude spectrum —Fn— for one standard tapping machine hammer at each excitation position, and the theoretical limits for the low frequency asymptotes (red stars).

Simulating the impact sound insulation

Impact sound insulation was simulated in the frequency domain using the force spectrum derived from the time domain with random phase shifts applied at five excitation points. The CLT floor was modelled in COMSOL as a 7-layer block, incorporating mechanical properties from Otani et al. (E_L = 8.5 GPa). Surface integration of the intensity beneath the floor yielded the radiated power, which was then used to calculate impact sound levels according to the formula from [8],

$$L_n = 10\log\left(\frac{\Pi_{rad}\ 4\rho c}{p_{ref}^2 A_0}\right), \tag{5}$$

where ρ and c are the density and speed of sound in air, respectively, $p_{ref} = 20 \cdot 10^{-6}$ is the reference pressure, A_0=10 m^2 is the reference absorption area and Π_{rad} is the radiated power. The radiated power was summed within each one-third octave band prior to this calculation. The simulated impact sound level are shown in Figure 9 along with measured impact sound levels of the same floor provided in [9].

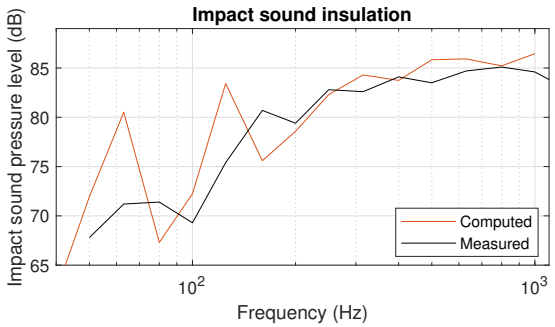

Figure 9: The simulated impact sound level using the total loss factor from [9] for the cross-laminated timber material in COMSOL. Additionally, the measured values also from [9] in black.

Overall, a decent fit was obtained for the general frequency range, however two peaks at the low frequencies are deviating significantly from the measured values.

The finite element model's mesh was verified by testing different mesh generation types and resolutions for both the CLT, air and PML domain. None or only small changes were observed in the impact sound levels, and due to the heavy increase in computation time, the current mesh generation and resolution, being *free tetrahedral* and minimum five elements per smallest wavelength, was assessed to be sufficient.

To further investigate the deviating peaks at low frequencies, the radiated power with a 10 Hz resolution was investigated (Figure 10). The black vertical lines indicate the one-third octave band limits. Notably, the bands containing the deviating peaks, 63 Hz and 125 Hz, also exhibit higher radiated power compared to neighbouring one-third octave bands.

One possible explanation is that the 10 Hz resolution coincides with certain resonance frequencies. However, an eigenfrequency study revealed that multiple resonance frequencies align similarly with other 10 Hz components, suggesting that these particular frequencies radiate more energy than others. The underlying cause of this behaviour was not further investigated.

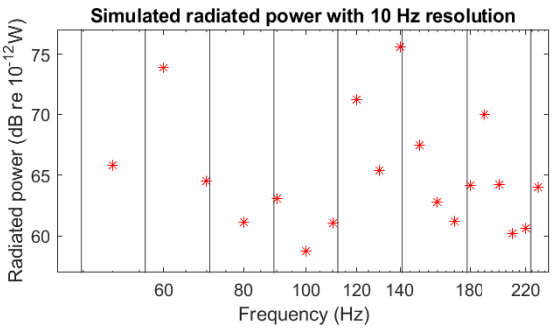

Figure 10: Simulated radiated power with a 10 Hz resolution (red stars). Vertical black lines visualise the one-third octave band limits, as it can be seen some one third octave bands includes more 10 Hz components than others.

Summary

The mechanical properties of a seven-layer CLT floor were investigated through experimental and computational modal analyses, which were compared with the MAC. After selecting material properties and simulating standard tapping machine excitation, the impact sound insulation of the CLT floor was computed, except for two deviating peaks in the low-frequency range. Further analysis revealed certain frequencies radiated more energy, causing these deviations. However, an eigenfrequency study showed no greater overlap between these frequencies and resonance frequencies compared to other frequency components, leaving the cause unresolved.

References

[1] Jæger, S. et al.: Acoustics and CLT - A study of airborne and impact sound in CLT slaps. Student report. The Technical University of Denmark. 2020.

[2] Liengaard, J. B. and Gotfredsen, M. F. et al.: Improving the sound insulation of existing wooden floor constructions – experiences from a laboratory study

[3] Gotfredsen, M. F.: Vibro-acoustic prediction model of impact sound insulation in cross-laminated timber floors. MA thesis. Technical University of Denmark, 2025.

[4] Mahoney W.: Wood Engineering Handbook (2nd Edition). BNI Building News, 2000.

[5] Otani,L. B. et al.: Determination of wood and byproducts elastic moduli using the impulse excitation technique.

[6] Brunskog, J. and Hammer, P.: The Interaction Between the ISO Tapping Machine and Lightweight Floors. In: Acta Acustica united with Acustica, Vol. 89 309-322 (2003).

[7] Lietzen, J. et al.: Simulation of impact force generated by an ISO tapping machine on a wooden slab using explicit dynamics analysis. In: Eng Struct 2022;270:114855 (2022).

[8] Brunskog, J. and Hammer, P.: Prediction Model for the Impact Sound Level of Lightweight Floors. In: Acta Acustica united with Acustica, Vol. 89 309-322 (2003).

[9] Liengaard, J. B.: Development of laboratory sound insulation measurement methods of cross-laminated timber elements. MA thesis. Technical University of Denmark, 2025.